BIOCHEMISTRY
including biophysical chemistry & molecular biology

Article

pubs.acs.org/biochemistry

A Complex Equilibrium among Partially Unfolded Conformations in Monomeric Transthyretin

Simona Conti,[†] Xinyi Li,[‡] Stefano Gianni,[§,∥] Seyyed Abolghasem Ghadami,[†] Joel Buxbaum,[‡] Cristina Cecchi,[†] Fabrizio Chiti,[†] and Francesco Bemporad*[,†]

[†]Dipartimento di Scienze Biomediche Sperimentali e Cliniche "Mario Serio", Sezione di Biochimica, Università degli Studi di Firenze, Viale G. B. Morgagni 50, 50134 Firenze, Italy

[‡]Department of Molecular and Experimental Medicine, The Scripps Research Institute, 10550 North Torrey Pines Road, MEM-230, La Jolla, California 92037, United States

[§]Istituto Pasteur Fondazione Cenci Bolognetti and Dipartimento di Scienze Biochimiche "A. Rossi Fanelli", Istituto di Biologia e Patologia Molecolari del CNR, Università di Roma "La Sapienza", P. le A. Moro 5, 00185 Roma, Italy

[∥]Department of Chemistry, University of Cambridge, Lensfield Road, Cambridge CB2 1EW, United Kingdom

Supporting Information

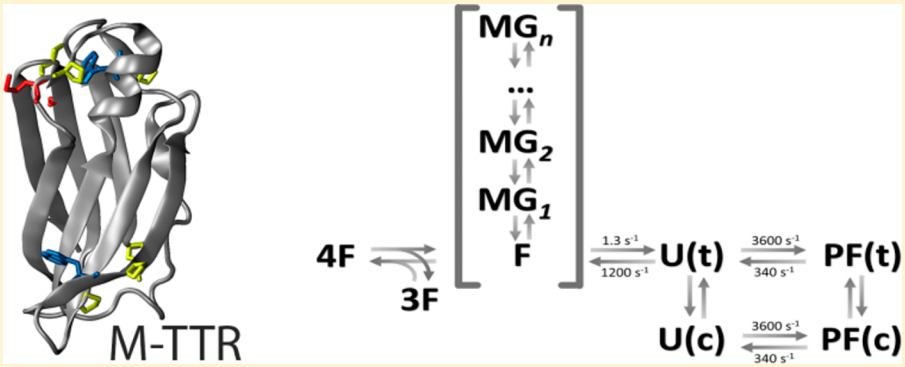

ABSTRACT: Aggregation of transthyretin (TTR) is known to be linked to the development of systemic and localized amyloidoses. It also appears that TTR exerts a protective role against aggregation of the Aβ peptide, a process linked to Alzheimer's disease. *In vitro*, both processes correlate with the ability of TTR to populate a monomeric state, yet a complete description of the possible conformational states populated by monomeric TTR *in vitro* at physiological pH is missing. Using an array of biophysical methods and kinetic tests, we show that once monomers of transthyretin are released from the tetramer, equilibrium is established between a set of conformational states possessing different degrees of disorder. A molten globular state appears in equilibrium with the fully folded monomer, whereas an off-pathway species accumulates transiently during refolding of TTR. These two conformational ensembles are distinct in terms of structure, kinetics, and their pathways of formation. Further subpopulations of the protein fold differently because of the occurrence of proline isomerism. The identification of conformational states unrevealed in previous studies opens the way for further characterization of the amyloidogenicity of TTR and its protective role in Alzheimer's disease.

Transthyretin (TTR) is a homotetrameric protein of 127 residues found in the cerebrospinal fluid (CSF) and serum.[1] The protein acts as a transporter of thyroid hormone thyroxine (T_4) and holo-retinol binding protein. While TTR is the primary carrier of T_4 in CSF, the protein acts as a backup carrier in serum, where the principal transporters are thyroid binding globulin and albumin.[1]

Despite its biological function as a carrier protein, TTR has been the subject of intense studies for more than 30 years because of its pathogenic properties. TTR can misfold and self-assemble into amyloid aggregates, leading to tissue dysfunction.[1−3] This process is linked to a series of sporadic and inherited pathological conditions,[2,3] including senile systemic amyloidosis, familial amyloid cardiomyopathy, familial amyloid polyneuropathy, and leptomeningeal amyloidosis. In these disorders, TTR aggregates in specific tissues, leading to a well-defined diseased phenotype probably caused by the formation of oligomeric species and subsequently of the amyloid and amorphous deposits.[4−7] More than 100 mutations have been linked to TTR pathologies, and a general trend is that the more the mutation destabilizes the quaternary structure, the more pathological the variant is.[1,8,9] The stability of the tetrameric structure has been linked to the kinetics of tetramer

Received: April 9, 2014
Revised: June 19, 2014
Published: June 19, 2014

   dx.doi.org/10.1021/bi500430w | *Biochemistry* 2014, 53, 4381−4392

dissociation. For instance, the V122I variant TTR exhibits fast dissociation kinetics because it forms a relatively unstable tetramer, but its monomers are as stable as those of wild-type TTR.[10] Conversely, T119M TTR (as well as the native murine TTR tetramer) has a dissociation rate lower than that of the wild-type protein, and inclusion of a T119M subunit into a tetramer otherwise composed of disease-associated subunits results in a higher kinetic barrier for tetramer dissociation and in the consequent protection of individuals from amyloidogenesis.[11] Thus, the kinetically destabilized tetramer is subject to dissociation, and the released monomeric TTR rapidly misfolds into a conformation that is competent for amyloid formation.[12−14] Once the aggregation competent state is formed, amyloid formation by TTR is an energetically favored process, rate-limited by low activation barriers for bimolecular association of misfolded TTR oligomers and monomers.[1,15] Remarkably, it was shown that TTR can be toxic even as a misfolded monomer.[4]

Somewhat counterintuitively, evidence is mounting that TTR can exert a protective role against amyloid fibril formation by the amyloid-β peptide (Aβ), whose aggregation is believed to be the cause of Alzheimer's disease (AD).[15−19] Such an effect is corroborated by evidence *in vivo* showing that co-expression of Aβ and TTR suppresses amyloid plaque formation and the pathological phenotype induced by Aβ.[20−22] *In vitro*, TTR was shown to bind to all forms of Aβ, including monomers, oligomers, and fibrils, although the affinity of binding is higher for Aβ oligomers, aggregates, and fibrils than for Aβ monomers.[18,21,23] The binding is highly dependent on the quaternary structure of TTR, with monomeric TTR binding Aβ with higher affinity than tetrameric TTR.[17,18] TTR was also shown to bind to preformed Aβ oligomers and HypF-N oligomers and reduce their toxicity, with such an ability being strongest for the monomeric form of TTR.[24,25]

The implication emerging from the pieces of evidence described above is that while the physiological function of TTR is linked to the packing of its folded state into a well-defined quaternary structure, different monomeric TTR conformations may play other biological roles, be they negative and pathological or positive and protective. Although tetrameric TTR is far more populated *in vivo* than the monomer, small amounts of misfolded monomers may be sufficient to trigger aggregation, while the interaction of monomeric TTR with its target may shift the equilibrium between tetramers and monomers toward the latter. Consequently, the elucidation of the different monomeric conformational states that can be populated by TTR represents a crucial step toward understanding the properties of the protein and the relationships between those properties and its *in vivo* function. Despite the large body of literature that can be found about the structure and dynamics of the TTR amyloidogenic state under nonphysiological conditions,[12−14,26−30] a complete description of the possible conformations populated by the protein at physiological pH values is still missing. This is in part due to the fact that kinetic and thermodynamic studies of TTR are complex following the existing equilibrium between the monomer and tetramer and the high stability of the tetrameric form at physiological pH values, which renders all monomeric conformations poorly populated.[31] In addition, the folding process of this protein from the fully unfolded to the fully folded state has not been studied in any detail, again because of the concomitant conversion of the monomer to the tetramer that raises complexities in the experimental studies that aimed to elucidate the folding process.

Such a lack of knowledge limits our understanding of the amyloidogenic properties of TTR as protein folding studies have often revealed partially folded amyloidogenic states.[32,33] To overcome this problem, we have focused our attention on the F87M/L110M double mutant of TTR (M-TTR). These mutations are located in crucial positions for tetramerization (Figure 1). Gel filtration, analytical centrifugation,[34] and cross-linking studies showed that M-TTR is 95% monomeric in the concentration range of 7−100 μM.[8,23,34] Urea-induced denaturation of M-TTR revealed that the mutant is not destabilized relative to the wild-type protein and the structure of the mutant is very similar to that of the wild-type protein, with some small differences observed in strands F−H.[34,35] Furthermore, it was shown that the conformational stability of M-TTR does not depend on protein concentration,[36] ruling out the existence of significant intermolecular processes such as aggregation and tetramerization. M-TTR is prone to aggregate at low pH and has been largely employed as a model to characterize the aggregation and trafficking of TTR.[8,9,34,36,37] Hence, M-TTR offers unique opportunities to investigate the equilibrium between folded and possible partially and fully unfolded conformations established by TTR, at physiological pH, once monomers have been released from the destabilized tetramer.

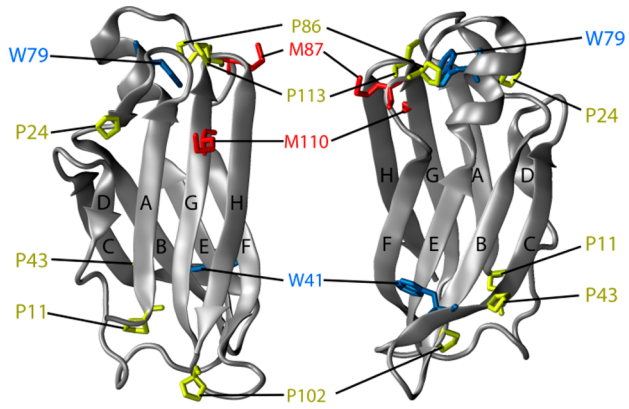

Figure 1. Front and back views of F87M/L110M TTR (M-TTR). Strands have been labeled to highlight topology. Mutated residues are colored red. Tryptophan side chains are colored blue. Proline residues are colored yellow. The figure was drawn using Protein Data Bank entry 1GKO.[34]

The availability of such a mutant allowed us to examine its folding mechanisms, which may also facilitate understanding of its misfolding. We have employed a battery of biophysical tools, including fluorescence, far- and near-UV CD, and DLS, and a number of experimental tools, including urea-induced denaturation curves, *T*-jump, stopped-flow kinetic, and thermal unfolding experiments, to investigate the thermodynamics and kinetics of the folding−unfolding process of M-TTR. The final goal of these experiments is the development of a model for the folding process of TTR and the identification of possible hidden partially folded states transiently populated along the folding pathway.

MATERIALS AND METHODS

Materials and Experimental Conditions. 8-Anilino-1-naphthalenesulfonic acid (ANS), dithiothreitol (DTT), human

dx.doi.org/10.1021/bi500430w | *Biochemistry* 2014, 53, 4381−4392

and bovine cyclophilin A, and urea were purchased from Sigma-Aldrich. In our study, the engineered monomer of human TTR (M-TTR) bearing the F87M and L110M mutations was prepared and purified in an *Escherichia coli* expression system as described previously.[34,38,39] Unless differently specified, all experiments in this work were conducted in 50 mM phosphate, 150 mM NaCl, and 2 mM DTT (pH 7.4) (hereafter termed phosphate buffer), at 37 °C.

Thermal Unfolding Experiments. Thermal unfolding measurements were conducted following the CD signal emitted by M-TTR at 216 nm using a Jasco (Tokyo, Japan) J-810 spectropolarimeter equipped with a thermostated cell holder attached to a Thermo Haake (Karlsruhe, Germany) C25P water bath. Thermal unfolding was achieved by heating the protein sample from 25 to 80 °C in a 1 mm path length quartz cell at a rate of 1 °C/min. The sample was then kept at this temperature for 20 min and subsequently cooled to 25 °C at a rate of 1 °C/min. Conditions were 29.1 μM M-TTR in phosphate buffer. The reversibility of the unfolding transitions was checked by measuring the CD signal at room temperature upon cooling after the end of the transition. Each spectrum was recorded as the average of many scans, blank-subtracted, and smoothed.

Dynamic Light Scattering (DLS) Measurements. DLS measurements were performed using a Zetasizer Nano S device from Malvern Instruments (Malvern, Worcestershire, U.K.) thermostated with a Peltier system. Low-volume 12.5 mm × 4.5 mm disposable cells were used. The refractive index and viscosity of phosphate buffer were calculated using the software provided with the instrument; a refractive index of 1.45 was used for M-TTR. Samples were prepared at a final protein concentration of 29.1 μM in phosphate buffer. Before the measurements, the protein sample was heated from 25 to 80 °C, maintained at this temperature for 20 min, subsequently cooled to 25 °C, and filtered with an anotop filter having a cutoff of 20 nm. The protein concentration was 29.1 μM. The presented size distributions were the average of three consecutive measurements.

Equilibrium Unfolding Experiments. Equilibrium denaturation studies were performed exploiting tryptophan fluorescence and CD in the near-UV and far-UV regions as probes. Twenty-eight to 34 samples were prepared containing M-TTR in phosphate buffer with urea at concentrations ranging from 0 to 7.6 M. Measurements were taken at 37 °C. Resulting plots were analyzed with the method provided by Santoro and Bolen[40] to obtain quantitative measurements of the free energy change upon denaturation in the absence of denaturant ($\Delta G^{H_2O}_{U-F}$), the concentration of middle denaturation (C_m), and the dependence of the free energy change upon denaturation on urea concentration (m).

In the case of fluorescence, spectra from 300 to 450 nm (excitation at 280 nm) were acquired for 28 equilibrated samples containing 2.9 μM M-TTR. A 10 mm × 2 mm quartz cuvette was used. Spectra were acquired using a PerkinElmer (Waltham, MA) LS 55 instrument. The signals at 358 and 313 nm were used to analyze the collected data as previously described.[34]

CD spectra from 200 to 260 nm were also acquired for 34 equilibrated samples using a Jasco J-810 spectropolarimeter. To reduce the urea absorbance below 210 nm and maximize the signal-to-noise ratio in this region, we acquired spectra using a 0.01 cm path length cuvette (Hellma) at 150 μM M-TTR. Thirty-two scans were averaged for each sample. All spectra were truncated after the high-tension (HT) voltage applied by the spectropolarimeter reached a value of 700 V: above this value light absorption rendered the signal-to-noise ratio too low. The mean residue ellipticity at 219 nm was calculated and plotted versus urea concentration.

CD spectra were also measured from 275 to 300 nm for 28 equilibrated samples containing 145.5 μM M-TTR. The Jasco J-810 spectropolarimeter was used with a 0.1 mm path length cuvette. The mean residue ellipticity at 290 nm was calculated and plotted versus urea concentration.

Stopped-Flow Kinetics Coupled to Intrinsic Fluorescence. Unfolding and refolding reactions were followed using a Bio-Logic (Claix, France) SFM-3 stopped-flow device equipped with an FC-15 cuvette and coupled to a fluorescence detection system. An excitation wavelength of 280 nm and a band-pass filter for monitoring emitted fluorescence above 320 nm were used. All the experiments were performed in phosphate buffer at 37 °C, at final protein concentrations of 1.5−2.9 μM. For the unfolding experiments, native M-TTR was diluted into solutions containing urea at final concentrations ranging from 3.5 to 6.5 M. Refolding reactions were initiated by a 10-fold dilution of the urea denatured protein into solutions containing low concentrations of urea. Final urea concentrations ranged from 0.2 to 3.5 M. The dead time was generally 10.4 ms.

In another set of experiments, the equilibrium signal measured at the end of unfolding kinetics was plotted versus urea concentration to linearly extrapolate the fluorescence of the unfolded protein under native conditions.

***T*-Jump Experiments.** Relaxation kinetics was measured as a function of urea concentration by using a Hi-Tech PTJ-64 capacitor-discharge *T*-jump apparatus (Hi-Tech). The temperature was rapidly changed from 28 to 37 °C. Ten to 20 individual traces were averaged at given denaturant concentrations. The protein concentration was typically 29.1 μM. The dead time ranged from 0.1 to 0.8 ms. The excitation wavelength was 280 nm, and the fluorescence emission was measured using a 320 nm cutoff glass filter.

Kinetic Analysis. Unfolding and refolding traces were fit to multiexponential functions to determine the rate constants of unfolding and folding, together with their relative amplitudes. The fitting procedure was made using the general equation

$$y(t) = mt + q + \sum_{i=1}^{n} A_i \exp(-\lambda_i t) \quad (1)$$

where $y(t)$ is the fluorescence signal recorded as a function of time, t is the time, A_i and λ_i are the apparent amplitude and rate constant of the ith phase, respectively, q is the fluorescence value at equilibrium, m is the dependence of equilibrium fluorescence on time, and n is the number of observed phases.

We then plotted the apparent rate constants of the major refolding phase (λ_2) observed in stopped-flow kinetics together with the rate constants obtained from *T*-jump experiments (λ_1). The logarithm of each rate constant was assumed to vary linearly with denaturant concentration. The observed chevron plots were fit globally with shared m values using three-state on-pathway and off-pathway models.[41] Values of λ_1 were also analyzed with a two-state model.[42] In the latter case, refolding rate constants in the absence of denaturant were linearly extrapolated from unfolding kinetics at high urea concentrations. The free energy change upon denaturation in the absence of denaturant ($\Delta G^{H_2O}_{U-F}$) was obtained from equilibrium unfolding. The global fit was obtained with Prism (GraphPad).

dx.doi.org/10.1021/bi500430w | *Biochemistry* 2014, 53, 4381−4392

Values obtained from this analysis were then used to run numerical simulations of the refolding process with COPASI and to calculate the equilibrium concentrations of each species.

Stopped-Flow CD. Folding of M-TTR was also monitored by far-UV CD at 219 nm using a Bio-Logic SFM-20 stopped-flow device coupled to the Jasco J-810 CD detection system described previously. Final conditions were 0.585 M urea in the phosphate buffer at 37 °C, at a protein concentration of 14.5 μM. The dead time of the experiment was 19 ms. The signal of the buffered solution with no protein was subtracted from the averaged trace. In the same experiment, the CD signal of the unfolded protein was measured at different urea concentrations to extrapolate the signal of the unfolded protein under native conditions.

Stopped-Flow ANS. Kinetic measurements were performed in the presence of ANS using the Bio-Logic SFM-3 stopped-flow device. An excitation wavelength of 370 nm and a band-pass filter for monitoring emitted fluorescence above 475 nm were used. All the experiments were performed in phosphate buffer with 100 μM ANS and 0.5 M urea (pH 7.4) at 37 °C and a final protein concentration of 2.91 μM.

Double-Jump Experiments. Two sets of double-jump experiments were employed. Interrupted refolding experiments were conducted on an Applied Photophysics (Leatherhead, U.K.) DX-17MV stopped-flow instrument with double-jump facility to assess the time dependence of accumulation of the native state. Refolding (first jump) and unfolding (second jump) were initiated by a symmetric mixing of the denatured and native protein with the appropriate buffer. In the first jump, 16 μM M-TTR denatured in 3 M urea with 2 mM DTT at pH 3.2 was diluted 1:1 into a phosphate buffer (pH 7.4) to a final urea concentration of 1.5 M. After a given delay time, the resulting solution obtained at the end of the first jump was diluted 1:1 into another solution containing 8.5 M urea (pH 7.4) to achieve denaturation at a final urea concentration of 5 M. Final conditions were 4 μM M-TTR, 5 M urea, and phosphate buffer (pH 7.4). The delay time ranged from 12 to 350 ms. The dead time was 6 ms. The excitation wavelength was 280 nm, and the fluorescence emission was measured using a 320 nm cutoff glass filter.

Interrupted unfolding experiments were performed with the Bio-Logic SFM-3 stopped-flow instrument to assess the occurrence of X−Pro peptide bond isomerism during refolding. In the first jump, 55 μM M-TTR in 1 M urea was diluted 1:4 into a buffer containing 6 M urea to a final urea concentration of 5 M. After the delay time, the resulting solution was diluted 1:4 into phosphate buffer. Final conditions were 2.2 μM M-TTR, 1 M urea, and phosphate buffer (pH 7.4). The delay time ranged from 44 ms to 30 s, while the dead time was 10.4 ms.

Folding in the Presence of CypA. Folding of M-TTR was studied in the presence of human and bovine CypA on the Bio-Logic SFM-3 stopped-flow apparatus by monitoring the intrinsic fluorescence emission above 320 nm with an excitation wavelength of 280 nm. Folding was initiated at 37 °C by mixing 21.8 μM TTR denatured in 5 M urea into a refolding buffer containing phosphate buffer and 0.5 M urea (pH 7.4) and CypA concentrations ranging from 0 to 0.67 μM. Obtained traces were fit to eq 1.

RESULTS

Thermal Denaturation of M-TTR Is an Irreversible Process. To characterize the unfolding−refolding pathway of M-TTR, we first studied thermal unfolding of the protein in 50 mM phosphate, 150 mM NaCl, and 2 mM DTT (pH 7.4) (hereafter termed phosphate buffer) by means of far-UV CD spectroscopy. While the CD spectrum at 25 °C before denaturation resembled that previously reported for folded M-TTR[34] (Figure 2A), the CD spectrum recorded at 79 °C

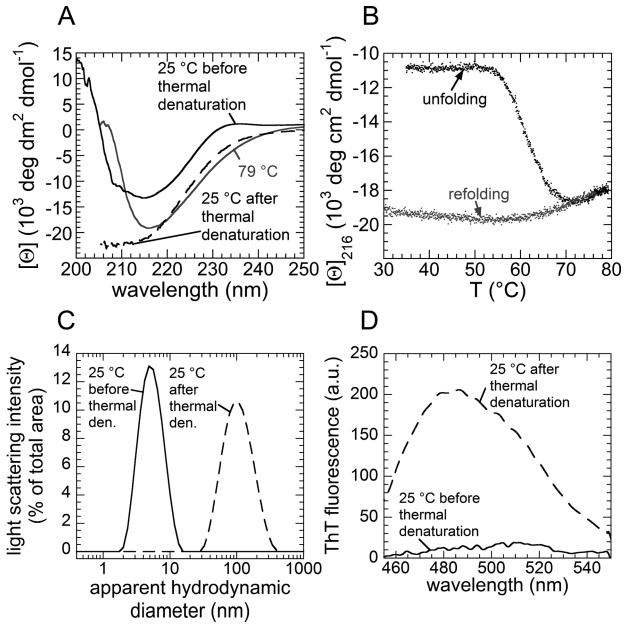

Figure 2. Thermal denaturation of M-TTR. (A) CD spectra of M-TTR recorded at different temperatures. Spectra are shown for the protein at 25 °C before (solid black line) and after (dashed black line) thermal unfolding and for thermally unfolded protein at 79 °C (solid gray line). (B) CD signal at 216 nm vs temperature during unfolding (black) and refolding (gray). (C) DLS distribution of M-TTR before (solid line) and after (dashed line) thermal denaturation. (D) Thioflavin T (ThT) fluorescence measured at 25 °C in the presence of M-TTR before (solid line) and after (dashed line) thermal unfolding.

revealed an increase in β-sheet structure content, as suggested by the signal at 216 nm (Figure 2A), and possible sample aggregation and precipitation, as suggested by an increase in the HT voltage applied to the photomultiplier of the spectropolarimeter, which was due to scattering of the light passing through the sample (not shown). The irreversibility of thermal denaturation was further confirmed by differences observed between CD spectra recorded at 25 °C before and after thermal denaturation, which revealed, following denaturation, a misfolded conformational ensemble possessing some degree of β-sheet structure and an increase in the number of disordered segments (Figure 2A). We followed the signal at 216 nm, where the largest difference between the signal at 25 and 79 °C was observed. The CD signal did not vary as the sample was heated to a temperature of 50 °C (Figure 2B). At higher temperatures, the protein underwent a transition, which was complete at 70 °C in our experimental setup. However, when the sample was cooled to 25 °C, the CD signal did not recover the initial value (Figure 2B).

To gain insight into this thermally unfolded state, we investigated the process by means of DLS. DLS analysis revealed that M-TTR is predominantly monomeric before thermal denaturation, with an apparent hydrodynamic diameter of 4.5 ± 1.0 nm, corresponding to a hydrodynamic radius of 2.25 ± 0.5 nm (Figure 2C). This value is compatible, within

dx.doi.org/10.1021/bi500430w | Biochemistry 2014, 53, 4381−4392

experimental error, with previously reported values of 1.9 nm[43] and 1.95 nm[34] and with the radius expected for a folded monomeric unit of TTR, as determined with X-ray crystallography, shielded by a water shell.[34] By contrast, M-TTR was converted into oligomers exhibiting an apparent hydrodynamic diameter of ~100 nm after thermal denaturation and cooling (Figure 2C). Unlike native M-TTR, these aggregated particles bound the dye thioflavin T (ThT) (Figure 2D), a fact reminiscent of the presence of amyloid-like structure in the sample.[44] The same set of experiments was repeated in the presence of 1.5 M urea to verify whether small amounts of the denaturant might be able to inhibit aggregation. Again, the results showed that thermal denaturation of M-TTR is irreversible even in the presence of urea (Figure S1 of the Supporting Information).

Urea-Induced Denaturation of M-TTR Revealed a Molten Globule. Given the difficulties associated with studying M-TTR unfolding by means of thermally induced denaturation, we investigated the process by urea equilibrium titration experiments. Different probes were used for the analysis, namely, CD in the far-UV region to assess secondary structure changes and CD in the near−UV region and tryptophan fluorescence to investigate tertiary structure. Spectra at urea concentrations ranging from 0 to 7.6 M obtained with the three spectroscopic probes are shown in Figure 3A−C; the corresponding unfolding traces (spectroscopic signal vs urea concentration) are shown in Figure S2A−E of the Supporting Information, while the corresponding native fraction plots are shown in Figure 3D. To maximize the signal-to-noise ratio, far-UV CD spectra were recorded by exploiting a 0.01 cm path length cuvette; each spectrum was truncated after the HT signal reached a value of 700 V, reflecting excessive light absorption in samples containing high urea concentrations (see Materials and Methods). All probes indicated a major cooperative unfolding transition taking place between 2 and 4 M urea, which leads to a conformational ensemble bearing tryptophan residues exposed to the solvent (Figure 3A) lacking persistent tertiary structure (Figure 3C) and possessing a mixture of β-sheet and disordered secondary structure (Figure 3B). Equilibrium unfolding traces were analyzed with a two-state transition model[40] to determine thermodynamic parameters associated with the conversion of the folded state (F) into the unfolded (U) state (Figure 3D,E). Interestingly, the use of different probes revealed variability in terms of concentrations of middle denaturation (C_m), reflecting different susceptibilities to denaturant of distinct structural elements (Figure S2 of the Supporting Information) and suggesting structural plasticity in the M-TTR native state. Thus, while fluorescence at 313 nm (Figure S2A of the Supporting Information) and CD at 290 nm (Figure S2D of the Supporting Information) point to a C_m located between 3.3 and 3.5 M, fluorescence at 358 nm (Figure S2B of the Supporting Information) and CD at 219 nm (Figure S2C of the Supporting Information) reveal a C_m around 3.0 M. M-TTR possesses two tryptophan residues contributing to the near-UV CD and fluorescence spectra and differing for their hydrophobic burial (Figure 1). Consequently, the observed variability may arise from a different resistance to denaturation of core and noncore regions. The analysis yielded values of conformational stability in the absence of denaturant ($\Delta G_{U-F}^{H_2O}$) of 6.4 ± 0.6, 4.9 ± 0.3, 4.8 ± 0.4, and 5.1 ± 0.3 kcal mol^{-1} for fluorescence at 313 and 358 nm, far-UV CD (219 nm), and near-UV CD (290 nm), respectively, and m values of 1.84 ± 0.20, 1.65 ± 0.10, 1.63 ± 0.12, and 1.55 ± 0.10 kcal mol^{-1} M^{-1} for fluorescence at 313 and 358 nm, far-UV CD (219 nm), and near-UV CD (290 nm), respectively. The weighted mean $\Delta G_{U-F}^{H_2O}$ and m values are 5.1 ± 0.2 kcal mol^{-1} and 1.61 ± 0.10 kcal mol^{-1} M^{-1}, respectively. These values are in reasonable agreement with those from similar experiments previously conducted under slightly different conditions.[34,36]

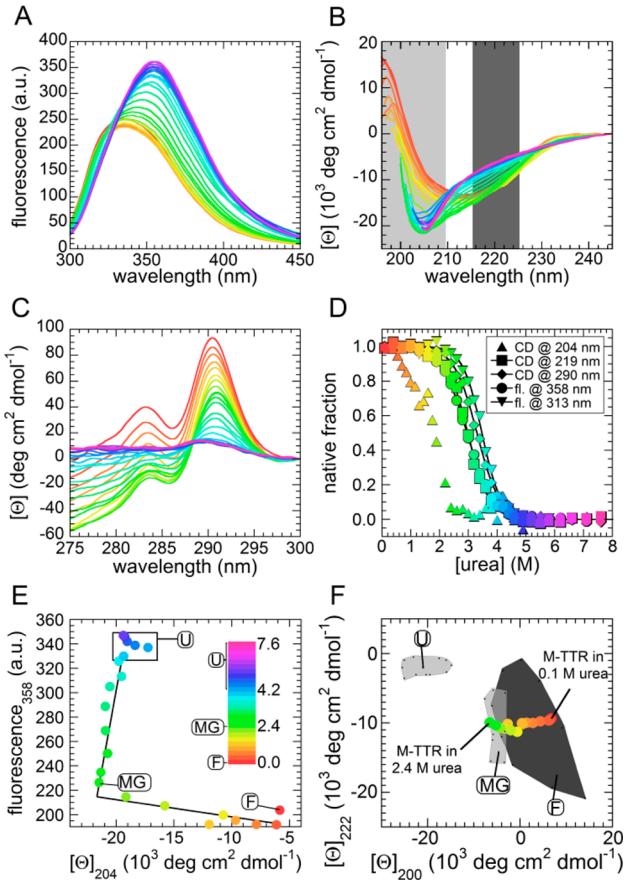

Figure 3. Urea-induced denaturation of M-TTR, followed with several spectroscopic probes. The color scale refers to urea concentration according to the legend displayed in panel E. (A) Equilibrium unfolding followed by intrinsic (tryptophan) fluorescence. (B) Equilibrium unfolding followed by far-UV CD, revealing two transitions: transition 1 is visible from 195 to 205 nm (light gray), and transition 2 is visible at 215−225 nm (dark gray). (C) Equilibrium unfolding followed by near-UV CD. (D) Native fraction as measured from best fits to a two-state model of data reported in panels A−C. Tryptophan fluorescence at 358 (●) and 313 nm (▼) and CD at 219 (■) and 290 nm (◆) indicated a cooperative transition between 2 and 4 M urea, whereas CD at 204 nm illustrated a noncooperative transition occurring between 0 and 2.4 M urea (▲). (E) Phase diagram[45] consisting of the plot of tryptophan fluorescence at 358 nm vs CD signal at 204 nm. This analysis suggested two transitions: (i) a transition from a fully folded state to a molten globular (MG) state and (ii) conversion of MG into an unfolded (U) state. (F) Plot of the CD signal at 222 nm vs the signal at 200 nm. This analysis is able to distinguish among folded (F), unfolded (U), and molten globular (MG) states.

Importantly, the analysis conducted with far-UV CD revealed the presence of a second transition located between 0 and 2.4 M urea and involving a remarkable change in CD signal between 195 and 210 nm (light gray region in Figure 3B). Comparison between near-UV and far-UV CD spectra of M-TTR in 0 and 2.4 M urea indicated that under the latter

dx.doi.org/10.1021/bi500430w | Biochemistry 2014, 53, 4381−4392

condition the protein experiences a slight increase in the mobility of aromatic side chains and exhibits a decrease in β-sheet content and an increase in random coil structure content. Such a transition involving the F state and a hidden conformation could be investigated by plotting the signal at 204 nm versus the urea concentration (Figure 3D and Figure S2E of the Supporting Information). The obtained plot illustrates a second transition, which is well separated from the first (Figure 3D and Figure S2E of the Supporting Information). An exhaustive analysis of the thermodynamic parameters showed that the concentration at middle denaturation (C_m) strongly depended on wavelength (Figure S3 of the Supporting Information). This is reminiscent of a non-cooperative transition. Although this effect might reflect the low signal-to-noise ratio observed below 200 nm, which limits the possibility of obtaining information at urea concentrations higher than 2 M, these data do not allow the assignment of the transition as a cooperative one.

Thus, the two transitions can be recapitulated by a phase diagram approach;[45] indeed, the plot of a spectroscopic probe able to detect the first transition (e.g., fluorescence at 358 nm) versus a second probe able to detect the second transition (CD at 204 nm) illustrates that a hidden conformational state forms along the unfolding pathway of M-TTR and is maximally populated at 2.4 M urea (Figure 3E). After the denaturation of the hidden conformational state, the unfolded state becomes populated. Similar results could be obtained by plotting different probes, e.g., tryptophan fluorescence at 358 nm versus CD at 276 nm (Figure S4 of the Supporting Information).

To characterize the conformational ensemble dominant at 2.4 M urea, we plotted the CD signal at 222 nm versus the signal at 200 nm (Figure 3F). It was reported that such an analysis is able to distinguish among folded, unfolded, and molten globular (MG) states.[46] In the case of M-TTR, the analysis revealed that, as the denaturant concentration increases from 0 to 2.4 M, the protein moves from a folded zone to a predominantly molten globular region (Figure 3F). This interpretation was corroborated by near-UV CD spectra, which showed a slight decrease in the magnitude of the tryptophan peak at 290 nm and that of the tyrosine peak at 283 nm (Figure 3C and Figure S2C of the Supporting Information), a fact reminiscent of the increased mobility of aromatic side chains.[47] Thus, it appears that the F state is in equilibrium with MG at denaturant concentrations lower than those required for complete denaturation.

Folding and Unfolding Kinetics Revealed a Transiently Populated State. We investigated the folding and unfolding kinetics of M-TTR using a stopped-flow device coupled to fluorescence or CD detection systems. Folding kinetics in the presence of 0.5 M urea involved a decrease in tryptophan fluorescence as M-TTR underwent refolding (Figure 4A). Such a decrease was complete after ~50 ms in 0.5 M urea. We gauged the signal of the unfolded protein under native conditions by linear extrapolation from measurements at high urea concentrations, where the protein is 100% unfolded (not shown). This analysis revealed that the fluorescence of the unfolded state is significantly different than the signal at the beginning of the refolding kinetics. This suggested the occurrence of one further refolding phase within the dead time of our stopped-flow experiments (Figure 4A). We will refer to the rate constant of the fast phase occurring in the dead time of our stopped-flow experiments as λ_1 and to the rate constant of the major refolding phase as λ_2 (λ_2 = 80 s^{-1} in the

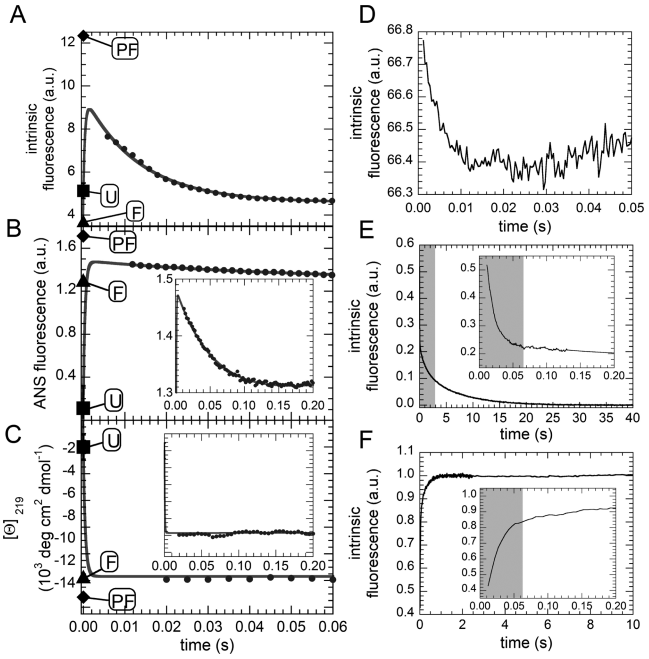

Figure 4. M-TTR refolding and unfolding kinetics, followed by means of different spectroscopic probes. (A–C) M-TTR refolding kinetics monitored by different techniques: tryptophan fluorescence (A), ANS binding (B), and far-UV CD (C). In each panel, the spectroscopic probe was monitored in stopped-flow refolding experiments at 0.25 M urea. Signal for the folded (F), partially folded (PF), and unfolded (U) states are shown. Insets show the same kinetics up to 200 ms. (D) *T*-jump relaxation kinetics at 2.5 M urea illustrates the presence of a fast phase (λ_1), complete in ~10 ms. (E) Refolding kinetics in phosphate buffer with 0.5 M urea show that after λ_1 and λ_2 are complete (gray zone in the inset) two slow phases can be detected, consisting of a further decrease in tryptophan fluorescence: λ_3, complete in ~2.5 s (gray zone in the main panel), and λ_4, complete in ~40 s. (F) M-TTR unfolding kinetics, showing the occurrence of two phases, which are complete in ~50 ms (gray zone in the inset, λ_1) and 1 s (λ_2).

absence of denaturant). The occurrence of the fast λ_1 phase was further confirmed by other spectroscopic probes, such as ANS binding to characterize exposure to solvent of hydrophobic clusters (Figure 4B) and far-UV CD to assess secondary structure content (Figure 4C). The conformational state populated at the beginning of the refolding kinetics exhibited a level of ANS binding higher than that of the unfolded state (Figure 4B). This is reminiscent of hydrophobic clusters partially exposed to the solvent. Smaller values obtained for λ_2 under these conditions are likely to arise from a refolding process rate-limited by the release of ANS (Figure 4B). The CD signal did not vary during refolding, indicating that the conformational state at the beginning of the refolding kinetics has a secondary structure similar to that of the folded state (Figure 4C). However, a dramatic change took place within the dead time, as the unfolded state was found to lack any secondary structure (Figure 4C). Consequently, both ANS fluorescence and CD confirmed the occurrence of the fast λ_1 phase.

To obtain direct evidence of such a phase, we used *T*-jump relaxation experiments performed at different urea concentrations and using intrinsic tryptophan fluorescence as a probe. When M-TTR was placed in urea concentrations corresponding to the major equilibrium transition (such as in 2.5 M urea) and underwent a *T*-jump from 28 to 37 °C, the protein

dx.doi.org/10.1021/bi500430w | *Biochemistry* 2014, 53, 4381–4392

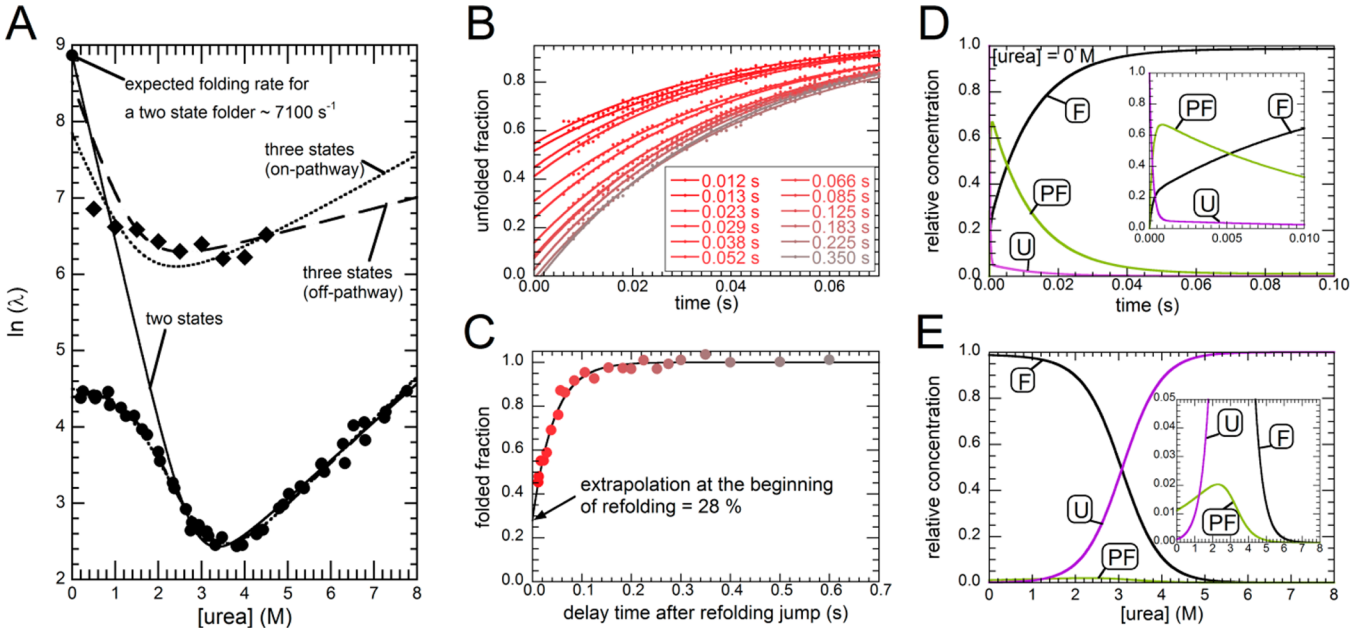

Figure 5. Characterization of the transiently populated state. (A) Natural logarithm of the observed folding−unfolding microscopic constants λ_1 (◆) and λ_2 (●), plotted as a function of urea concentration (chevron plot). The refolding limb of the chevron plot deviates from linearity at urea concentrations of <2 M, where a downward curvature, generally termed "rollover", is observed. The solid line represents the best fit of the data to the equation for a two-state transition.[42] Dashed and dotted lines represents best global fits to three-state off-pathway and on-pathway models, respectively.[41] (B and C) Interrupted refolding double-jump experiment. The protein unfolded in 3 M urea at pH 3.2 was first refolded by dilution into a refolding phosphate buffer at pH 7.4. After a given delay time, the protein was denatured in a second jump to 8.5 M urea at pH 7.4. (B) Experimental traces obtained at the indicated delay times. (C) Calculated folded fraction vs delay time. The amount of folded protein present at the beginning of the refolding experiment was extrapolated from a single-exponential fit. The color scale corresponds to the legend in panel B. (D and E) Transient (D) and equilibrium (E) concentrations for the folded (F, black line), unfolded (U, purple line), and partially folded (PF, blue line) states according to the off-pathway model at 0 M urea (D) and plotted vs urea concentration (E). Insets show magnifications to illustrate PF concentrations.

underwent a rapid decrease in fluorescence, which was complete in ~10 ms (Figure 4D). As expected, the time scale of this process was within the dead time of our stopped-flow experiments and was therefore masked. Hence, *T*-jump relaxation kinetics provided direct evidence of the formation of a transiently populated state. After λ_1 and λ_2 were complete, refolding of M-TTR followed by means of tryptophan fluorescence exhibited two more exponential phases (Figure 4E). The third and fourth phases were complete in ~2.5 s (λ_3 = 2 s^{-1}) and ~30 s (λ_4 = 0.15 s^{-1}), respectively.

As far as unfolding is concerned, the process, monitored at urea concentrations of >4 M by means of tryptophan fluorescence, involved an increase in fluorescence (Figure 4F). Two exponential phases could be distinguished. The first phase was complete in ~50 ms in 5 M urea (inset of Figure 4F), which is on the same time scale employed in similar experiments previously reported under slightly different conditions.[8] The second phase lasted ~5 s (Figure 4F).

The Transiently Populated State Is a Partially Folded Off-Pathway Ensemble. We built the chevron plot for M-TTR (Figure 5A). In particular, *T*-jump experiments were conducted in the urea concentration range 0.5−4.5 M to obtain the plot of ln(λ_1) versus urea concentration (◆ in Figure 5A). Rate constants for the major folding−unfolding transition (λ_2) were obtained from best fits of experimental kinetic traces to multiexponential equations, and these values were used to build the plot of ln(λ_2) versus urea concentration (● in Figure 5A). The C_m value obtained from the analysis of this plot, calculated as the urea concentration at which extrapolated refolding and unfolding rate constants are equal, was in good agreement with that determined for the MG → U transition observed at equilibrium. Indeed, kinetic and equilibrium experiments indicated C_m values of 3.20 ± 0.20 and 3.16 ± 0.20 M urea, respectively. However, a downward curvature could be observed in the folding limb of the plot. Such a deviation from the expected plot for a two-state folder[42] is usually termed rollover[48−50] and can be recapitulated in kinetic terms as follows. The extrapolated unfolding rate constant in the absence of denaturant was 1.82 s^{-1}. Given the conformational stability obtained by equilibrium experiments, the folding rate constant under the same conditions was calculated to be ~7100 s^{-1} for a two-state folder (Figure 5A). The refolding rate constant extrapolated by experimental data was approximately 81 s^{-1}, 2 orders of magnitude lower than the calculated value.

While rollover in the M-TTR chevron plot probably reflects the transient formation of a hidden conformation,[41] other interpretations were previously proposed for this phenomenon, including a Hammond effect[51] and aggregation artifacts.[52] We performed refolding kinetics at different M-TTR concentrations to detect possible aggregation phenomena occurring during refolding (Figure S5A,B of the Supporting Information). Indeed, any intermolecular process would be affected by varying protein concentrations. However, neither kinetic constants (Figure S5C of the Supporting Information) nor phase amplitudes (Figure S5D of the Supporting Information), obtained from best fits of experimental data to eq 1, significantly changed as the M-TTR concentration ranged from 0.5 to 5 μM, confirming that a conformational state different from the folded and unfolded states forms transiently during refolding of M-TTR.

dx.doi.org/10.1021/bi500430w | *Biochemistry* 2014, 53, 4381−4392

Table 1. Kinetic Data for the M-TTR Refolding Process, As Obtained from Best Fits of Experimental Data to On-Pathway and Off-Pathway Models

model	$k_{U\to PF}^{H_2O}$ (s^{-1})	$m_{U\to PF}$ (kcal mol^{-1} M^{-1})	$k_{PF\to U}^{H_2O}$ (s^{-1})	$m_{PF\to U}$ (kcal mol^{-1} M^{-1})	$k_{PF\to F}^{H_2O}$ (s^{-1})	$m_{PF\to F}$ (kcal mol^{-1} M^{-1})	$k_{F\to PF}^{H_2O}$ (s^{-1})	$m_{F\to PF}$ (kcal mol^{-1} M^{-1})	$k_{U\to F}^{H_2O}$ (s^{-1})	$m_{U\to F}$ (kcal mol^{-1} M^{-1})	$k_{F\to U}^{H_2O}$ (s^{-1})	$m_{F\to U}$ (kcal mol^{-1} M^{-1})
on-pathway (U ⇋ PF ⇋ F)	2400	0.84	130	0.21	93.0	1.0×10^{-11}	1.6	0.32	–	–	–	–
off-pathway (PF ⇋ U ⇋ F)	3600	1.07	340	0.090	–	–	–	–	1200	1.03	1.30	0.35

To assess whether the transiently populated state forming after the first fast phase of folding (λ_1) represented a true folding intermediate or rather a kinetic trap that is off the refolding pathway and slows the bulk process, we analyzed our chevron plot with on-pathway and off-pathway models.[41] Results of such analyses are shown in Figure 5A and summarized in Table 1. In principle, the analysis can discriminate between the two models because only the on-pathway model allows λ_2 to be higher than λ_1 in the absence of denaturant.[41,53] If the experimental analysis shows that λ_2 is higher than λ_1, the off-pathway model can be ruled out. However, in the case of M-TTR, both models successfully interpreted data. Consequently, while the analysis yielded all the kinetic parameters for the refolding of M-TTR and the transient and equilibrium concentrations of the species involved in the process, it was not conclusive in defining the folding pathway.

To shed light on the on- or off-pathway nature of the transiently populated state, we performed an interrupted refolding double-jump experiment.[54,55] In this experiment, M-TTR was first unfolded in 3 M urea at pH 3.2 (Figure S6 of the Supporting Information). It was then refolded in 1.5 M urea at pH 7.4 (first jump) and after a delay time unfolded back in 5 M urea at pH 7.4 (second jump). By varying the delay time after the first jump (refolding), one can vary the amount of protein undergoing unfolding in the second jump (unfolding), as described previously.[55,56] Consequently, this experiment allowed the relative amount of unfolded and native protein to be reconstructed during the refolding time (Figure 5B). The rationale behind the approach is that only in the off-pathway model can the amount of native protein after the first jump, and before the delay time starts, be greater than zero. Indeed, in an on-pathway model, all the protein needs to transit through the partially folded conformation to refold, and with a delay time of 0 s, no native protein is expected to be populated after the first refolding jump.[55] By contrast, in an off-pathway model, the protein can easily access the native state without passing through the partially folded state, and a significant amount of native protein may be populated after the first refolding jump with a delay time of 0 s. In the case of M-TTR, the amount of native protein extrapolated to a delay time of 0 s was 28% (Figure 5C). Consequently, the transiently populated state is an off-pathway kinetic trap. Only after its denaturation can the protein convert into the correctly folded state.

The kinetic constants obtained from the off-pathway model were thus used to calculate transient and equilibrium concentrations of F, U, and PF states (Figure 5D,E) and the spectroscopic signals of the PF state (Figure 4A– C). Results revealed that the transiently populated state is hyperfluorescent relative to the fully folded state (Figure 4A), a fact reminiscent of an environment surrounding tryptophan side chains where the level of quenching is lower. Furthermore, the transiently populated species exhibits stronger ANS binding than the fully folded state (Figure 4B). However, its CD signal at 219 nm is comparable to that of the native state (Figure 4C). Consequently, the transiently populated state can be described as a partially folded (PF) conformation possessing secondary structure globally comparable to those of the fully folded state, some hydrophobic clusters exposed to solvent, and some non-native contacts that must be dismantled before M-TTR can convert into the fully folded state.

Folding Slow Phases Arise from Proline Isomerism. Another important question to answer was the characterization of the two folding slow phases λ_3 and λ_4 (Figure 4E). The rate constants of such phases did not depend on urea concentration, suggesting that they could arise from proline isomerism.[57] M-TTR possesses eight X–Pro bonds (Figure 1), all populating a *trans* configuration in the folded state.[34,35] To test this hypothesis, we performed folding kinetics experiments in the presence of cyclophilin A (cypA), a peptidyl-prolyl isomerase that catalyzes the *cis–trans* interconversion of X–Pro peptide bonds.[57] While bovine cypA did not have any effect on M-TTR refolding (data not shown), human cypA was able to accelerate the process as the enzyme concentration increased from 0 to 0.6 μM (Figure 6A). Analysis of the traces revealed that λ_2 was not affected by the presence of cypA whereas slow phases (λ_3 and λ_4) were both significantly accelerated (Figure 6B).

To further confirm the occurrence of proline isomerism during M-TTR refolding, interrupted unfolding double-jump experiments were conducted. Briefly, M-TTR was first unfolded in 5 M urea and, after a delay time, refolded in 1 M urea. The rationale in this case is that by varying the delay time between the first (unfolding) and second (refolding) jump, one can vary the time the protein is allowed to refold. As proline isomerism requires several seconds to reach its equilibrium, slow phases are expected to undergo decreases in amplitude and eventually disappear as the delay time decreases. While the amplitude of the fast phase did not depend on delay time, those of the slow phases decreased as the delay time decreased (Figure 6C). The plot of the amplitudes versus delay time showed two exponential processes whose amplitudes satisfactorily extrapolated to 0.00 ± 0.02 (A_3) and 0.04 ± 0.02 (A_4) when the delay time is zero (Figure 6D). Kinetic constants obtained by fitting the values of A_3 and A_4 versus delay time to a single-exponential function were in reasonable agreement with the values obtained from single-jump refolding experiments under the same conditions. This corroborated the idea that both slow phases arise from proline isomerism. However, it should be noted that while λ_4 occurs on the typical time scale for proline isomerism, λ_3 appears to be too fast for such a process. It is therefore possible that only λ_4 should be attributed to proline isomerism, while results for λ_3 originate from the partial overlap of the two slow phases.

DISCUSSION

A Model for M-TTR Folding. In this work, we exploited a battery of biophysical methods and performed a number of kinetic tests to investigate the mechanisms of M-TTR refolding,

dx.doi.org/10.1021/bi500430w | *Biochemistry* 2014, 53, 4381–4392

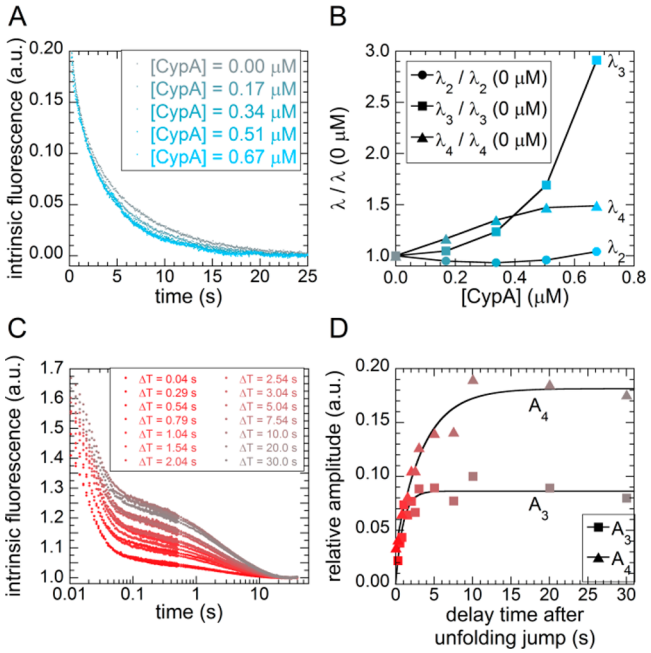

Figure 6. Characterization of M-TTR refolding slow phases (λ_3 and λ_4). (A) Effect of human CypA on M-TTR folding. The folding reaction was monitored in phosphate buffer containing 0.5 M urea, in the presence of increasing quantities of human CypA. The color scale refers to the cypA concentration, according to the table shown in the figure. (B) Microscopic refolding rate constants reported as ratios of the value obtained for the different phases in the presence of CypA and the corresponding value in its absence. The color scale corresponds to that in panel A. (C) Double-jump interrupted unfolding experiment. The protein was first denatured in a phosphate buffer to 5 M urea (first jump) and then, after a given delay time, refolded in a phosphate buffer to 1 M urea (second jump). The color scale refers to the delay time, according to the table shown in the figure. (D) Plot displaying phase relative amplitudes obtained from best fits of experimental data to eq 1 vs delay time. The color scale corresponds to that in panel C. These traces were analyzed with a single-exponential rise function (solid lines).

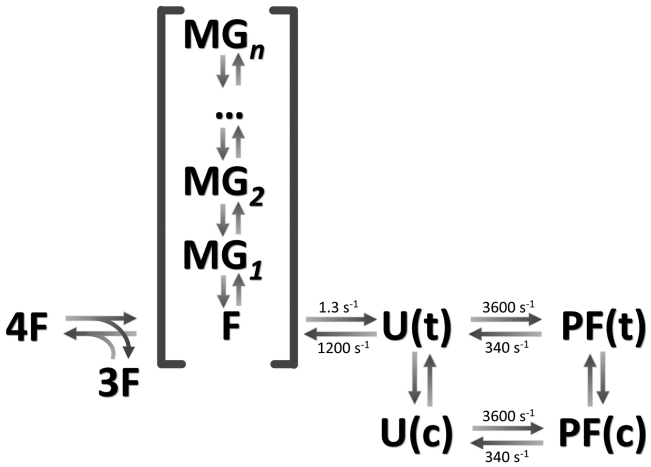

Figure 7. Model for the folding process of TTR. 4F defines the tetramer. F defines the folded monomer. MG_1, MG_2, ..., and MG_n correspond to a set of molten globular conformations. U(t) and U(c) refer to the unfolded state with one or more X−Pro peptide bonds in the *trans* and *cis* configurations, respectively. PF(t) and PF(c) refer to the partially folded state with one or more X−Pro peptide bonds in the *trans* and *cis* configurations, respectively. Rate constants for each phase are shown (see the text).

with the final goal of proposing a model for the process. Such a model is presented in Figure 7. Once a monomer of TTR (F) is released from the tetramer (4F), the protein establishes a complex equilibrium and can access a set of conformational ensembles. First, the protein can convert from the fully folded state (F) into an ensemble of molten globular conformations (MG_1, MG_2, ..., and MG_n) bearing increasing amounts of disorder. When compared to F, such an MG ensemble possesses enhanced mobility of aromatic side chains, a decrease in β-sheet structure content, and an increase in the number of random coil segments, in the presence of a substantially unaltered tertiary structure. Furthermore, the folded/molten globular ensemble is in equilibrium with the unfolded state (U).

However, before the unfolded state converts into F, a large subpopulation of the unfolded protein molecules experience a transient conversion into a kinetic trap consisting of a partially folded (PF) state. The PF state can be described as an ensemble of conformations exhibiting a secondary structure content comparable to that of the folded state but with a larger amount of hydrophobic clusters exposed to solvent compared to F. Notwithstanding that and given the off-pathway nature of PF, one can speculate that such an ensemble possesses at least a few non-native contacts that must be dismantled before M-TTR can convert into the correctly folded state F. One further conformational ensemble can be identified thanks to the characterization of the slow phases of folding. Indeed, we showed that refolding of a subpopulation of M-TTR is decelerated due to the incorrect (*cis*) configuration of one or more X−Pro peptide bonds; only after such bonds are converted into the right (*trans*) configuration can refolding proceed.

Importantly, the MG and PF states do not refer to the same conformational state, as revealed by differences between these two states in terms of structure, kinetics, and pathway of formation. (i) The MG ensemble can be observed in equilibrium experiments and is the dominant species at urea concentrations around 2.4 M (Figure 3). Conversely, our kinetic analysis illustrates that PF is populated only transiently. Its population at the equilibrium is not higher than 2% under the same conditions (Figure 5). (ii) MG is directly in equilibrium with F, and its formation precedes denaturation, whereas the PF ensemble must convert into U before accessing the F state. (iii) The transition from F to PF appears to be cooperative, while conversion of F into MG lacks cooperativity. (iv) MG and F are indistinguishable in terms of intrinsic fluorescence (Figure 3A and Figure S2A of the Supporting Information), while PF has a significantly higher fluorescence than F as assessed by our stopped-flow kinetics (Figure 4A), suggesting a different environment surrounding aromatic side chains. (v) CD analysis reveals that the secondary structure content of PF is globally nativelike, while MG bears disordered segments. Consequently, our identification of the PF and MG states illustrates two conformational ensembles that differ in terms of structure, dynamics, kinetics, and pathway of formation.

It is also important to point out the relative abundances of the PF and MG conformational ensembles. The PF state is populated only transiently: calculations based on kinetic data show that more than 1% of the protein populates the PF state at equilibrium in the absence of denaturant (Figure 5D). As far as the MG state is concerned, the lack of cooperativity displayed by the F → MG transition makes it difficult to

dx.doi.org/10.1021/bi500430w | *Biochemistry* 2014, 53, 4381−4392

quantify the amount of protein populating the MG state. However, data in Figure 3D suggest that the transition begins at very low urea concentrations. Consequently, the amount of protein experiencing a molten globular conformation may be significant even in the absence of denaturant, especially in the presence of destabilizing mutations.

Importance of Partially Folded States in TTR. Several decades of research of TTR have highlighted the importance of characterizing partially folded conformations populated by this protein. First, it is now clear that transient conformational fluctuations induce the conversion of the fully folded state of TTR into an ensemble of partially folded conformations that are prone to aggregation.[12−14] The characterization of this aggregation prone state is therefore crucial for understanding the mechanisms underlying TTR aggregation. Several investigations consisting of limited proteolysis and spectroscopic methods reported that the major event during the misfolding of monomeric TTR is the local unfolding and subsequent displacement of the two peripheral β-strands C and D (Figure 1) and the loop connecting them.[13,27−29] The dislocation of this edge region unmasks amyloid prone segments normally buried in the TTR folded state, and solvent exposure of these segments mediates the establishment of the intermolecular interactions that initiate aggregation.[29,58,59] More recently, it was proposed, by means of nuclear magnetic resonance relaxation dispersion experiments, that the amyloidogenic state of TTR possesses a largely nativelike CBEF sheet while the DAGH sheet is disrupted, especially in strands D and H.[30] This description is corroborated by molecular dynamics simulations suggesting that the CBEF sheet undergoes significant structural changes under conditions that promote aggregation.[60] Importantly, complete unfolding of TTR inhibits aggregation.[13] Thus, while the structural characteristics of the TTR amyloidogenic state must yet be clarified, there is consensus about the idea that such a state(s) must possess partial and local unfolding.

Second, evidence is accumulating that TTR may play a protective role against AD.[15−17,19−24,61] Different mechanisms have been proposed for such protective activity. These include direct facilitation of Aβ degradation,[62] transport of Aβ from the central nervous system to serum,[15] inhibition of Aβ aggregation[15−17,19−24] and suppression of Aβ oligomer toxicity.[24] While the mechanisms of the TTR-mediated protection against AD *in vivo* remain to be fully understood, it was recently proposed that *in vitro* interactions between TTR and Aβ can be mediated by either tetrameric or monomeric TTR, the two processes involving somewhat different mechanisms.[61] In both cases, it is reasonable that binding is mediated by a protein conformation that can bind peptide segments as hydrophobic as Aβ. In the TTR tetramer, this appears to be the highly hydrophobic T_4 binding site.[23] The more hydrophobic structure of the TTR monomer appears to allow it to interact with relatively small oligomers, rather than the monomer, in essence increasing its valence with respect to the Aβ monomer. This conformation is likely to be different from the fully folded state and display some extent of partial unfolding.

Therefore, the identification and characterization of partially folded states of TTR represents a crucial step toward understanding the peculiar properties of this protein. Here we show that once a monomer is released from tetrameric TTR, a complex equilibrium is established between the fully folded monomer and at least two partially folded states. A small yet significant population of the monomeric protein populates two conformational states distinct from the fully folded one and possessing some degree of improper or incomplete folding. Future studies will clarify whether such conformational states may play important roles with respect to the biological activity of TTR, both as a precursor of amyloid fibrils and as a protective agent against AD.

■ ASSOCIATED CONTENT

Supporting Information

Figures S1−S6 and related legends. This material is available free of charge via the Internet at http://pubs.acs.org.

■ AUTHOR INFORMATION

Corresponding Author

*Dipartimento di Scienze Biomediche Sperimentali e Cliniche "Mario Serio", Sezione di Biochimica, Università degli Studi di Firenze, Viale G. B. Morgagni 50, 50134 Firenze, Italy. E-mail: francesco.bemporad@unifi.it. Telephone: 0039-055-275-1211.

Funding

This study was supported by the Italian MIUR (FIRB Project RBFR109EOS and "Programma per giovani ricercatori Rita Levi Montalcini 2012" to F.B. and Progetto di Interesse 'Invecchiamento' to S.G.), the Fondazione Cassa di Risparmio di Pistoia e Pescia (Project 2012.0266) (C.C. an S.C.), and Sapienza University of Rome (C26A13T9NB to S.G.).

Notes

The authors declare no competing financial interest.

■ ACKNOWLEDGMENTS

We are thankful to Dr. Nunilo Cremades (University of Cambridge) for technical support and useful discussions.

■ ABBREVIATIONS

Aβ, amyloid-β peptide; AD, Alzheimer's disease; ANS, 8-anilino-1-naphthalenesulfonic acid; CD, circular dichroism; CSF, cerebrospinal fluid; cypA, cyclophilin A; DLS, dynamic light scattering; DTT, dithiothreitol; F, folded; HT, high-tension; M-TTR, monomeric transthyretin; MG, molten globule; PF, partially folded; T_4, thyroxine; ThT, thioflavin T; TTR, transthyretin; U, unfolded.

■ REFERENCES

(1) Johnson, S. M., Connelly, S., Fearns, C., Powers, E. T., and Kelly, J. W. (2012) The transthyretin amyloidoses: From delineating the molecular mechanism of aggregation linked to pathology to a regulatory-agency-approved drug. *J. Mol. Biol. 421*, 185−203.

(2) Buxbaum, J. N. (2007) Transthyretin and the Transthyretin Amyloidoses. In *Protein Misfolding, Aggregation, and Conformational Diseases* (Uversky, V. N., and Fink, A. L., Eds.) pp 259−283, Springer, Santa Cruz, CA.

(3) Fearns, C., Connelly, S., Powers, E. T., and Kelly, J. W. (2013) Development of Therapeutic Strategies for the Transthyretin Amyloidoses. In *Amyloid Fibrils and Prefibrillar Aggregates* (Otzen, D. E., Ed.) pp 373−394, Wiley-VCH, Weinheim, Germany.

(4) Reixach, N., Deechongkit, S., Jiang, X., Kelly, J. W., and Buxbaum, J. N. (2004) Tissue damage in the amyloidoses: Transthyretin monomers and nonnative oligomers are the major cytotoxic species in tissue culture. *Proc. Natl. Acad. Sci. U.S.A. 101*, 2817−2822.

(5) Sorgjerd, K., Klingstedt, T., Lindgren, M., Kagedal, K., and Hammarstrom, P. (2008) Prefibrillar transthyretin oligomers and cold stored native tetrameric transthyretin are cytotoxic in cell culture. *Biochem. Biophys. Res. Commun. 377*, 1072−1078.

(6) Sousa, M. M., Cardoso, I., Fernandes, R., Guimaraes, A., and Saraiva, M. J. (2001) Deposition of transthyretin in early stages of familial amyloidotic polyneuropathy: Evidence for toxicity of non-fibrillar aggregates. *Am. J. Pathol. 159*, 1993−2000.
(7) Sousa, M. M., Fernandes, R., Palha, J. A., Taboada, A., Vieira, P., and Saraiva, M. J. (2002) Evidence for early cytotoxic aggregates in transgenic mice for human transthyretin Leu55Pro. *Am. J. Pathol. 161*, 1935−1948.
(8) Hammarstrom, P., Jiang, X., Hurshman, A. R., Powers, E. T., and Kelly, J. W. (2002) Sequence-dependent denaturation energetics: A major determinant in amyloid disease diversity. *Proc. Natl. Acad. Sci. U.S.A. 99* (Suppl. 4), 16427−16432.
(9) Sekijima, Y., Wiseman, R. L., Matteson, J., Hammarstrom, P., Miller, S. R., Sawkar, A. R., Balch, W. E., and Kelly, J. W. (2005) The biological and chemical basis for tissue-selective amyloid disease. *Cell 121*, 73−85.
(10) Jiang, X., Buxbaum, J. N., and Kelly, J. W. (2001) The V122I cardiomyopathy variant of transthyretin increases the velocity of rate-limiting tetramer dissociation, resulting in accelerated amyloidosis. *Proc. Natl. Acad. Sci. U.S.A. 98*, 14943−14948.
(11) Hammarstrom, P., Wiseman, R. L., Powers, E. T., and Kelly, J. W. (2003) Prevention of transthyretin amyloid disease by changing protein misfolding energetics. *Science 299*, 713−716.
(12) Colon, W., and Kelly, J. W. (1992) Partial denaturation of transthyretin is sufficient for amyloid fibril formation in vitro. *Biochemistry 31*, 8654−8660.
(13) Lai, Z., Colon, W., and Kelly, J. W. (1996) The acid-mediated denaturation pathway of transthyretin yields a conformational intermediate that can self-assemble into amyloid. *Biochemistry 35*, 6470−6482.
(14) Quintas, A., Vaz, D. C., Cardoso, I., Saraiva, M. J., and Brito, R. M. (2001) Tetramer dissociation and monomer partial unfolding precedes protofibril formation in amyloidogenic transthyretin variants. *J. Biol. Chem. 276*, 27207−27213.
(15) Schwarzman, A. L., Gregori, L., Vitek, M. P., Lyubski, S., Strittmatter, W. J., Enghilde, J. J., Bhasin, R., Silverman, J., Weisgraber, K. H., Coyle, P. K., et al. (1994) Transthyretin sequesters amyloid β protein and prevents amyloid formation. *Proc. Natl. Acad. Sci. U.S.A. 91*, 8368−8372.
(16) Costa, R., Goncalves, A., Saraiva, M. J., and Cardoso, I. (2008) Transthyretin binding to A-β peptide: Impact on A-β fibrillogenesis and toxicity. *FEBS Lett. 582*, 936−942.
(17) Du, J., and Murphy, R. M. (2010) Characterization of the interaction of β-amyloid with transthyretin monomers and tetramers. *Biochemistry 49*, 8276−8289.
(18) Li, X., Zhang, X., Ladiwala, A. R., Du, D., Yadav, J. K., Tessier, P. M., Wright, P. E., Kelly, J. W., and Buxbaum, J. N. (2013) Mechanisms of transthyretin inhibition of β-amyloid aggregation in vitro. *J. Neurosci. 33*, 19423−19433.
(19) Liu, L., and Murphy, R. M. (2006) Kinetics of inhibition of β-amyloid aggregation by transthyretin. *Biochemistry 45*, 15702−15709.
(20) Link, C. D. (1995) Expression of human β-amyloid peptide in transgenic *Caenorhabditis elegans*. *Proc. Natl. Acad. Sci. U.S.A. 92*, 9368−9372.
(21) Choi, S. H., Leight, S. N., Lee, V. M., Li, T., Wong, P. C., Johnson, J. A., Saraiva, M. J., and Sisodia, S. S. (2007) Accelerated Aβ deposition in APPswe/PS1δE9 mice with hemizygous deletions of TTR (transthyretin). *J. Neurosci. 27*, 7006−7010.
(22) Buxbaum, J. N., Ye, Z., Reixach, N., Friske, L., Levy, C., Das, P., Golde, T., Masliah, E., Roberts, A. R., and Bartfai, T. (2008) Transthyretin protects Alzheimer's mice from the behavioral and biochemical effects of Aβ toxicity. *Proc. Natl. Acad. Sci. U.S.A. 105*, 2681−2686.
(23) Du, J., Cho, P. Y., Yang, D. T., and Murphy, R. M. (2012) Identification of β-amyloid-binding sites on transthyretin. *Protein Eng., Des. Sel. 25*, 337−345.
(24) Li, X., Masliah, E., Reixach, N., and Buxbaum, J. N. (2011) Neuronal production of transthyretin in human and murine Alzheimer's disease: Is it protective? *J. Neurosci. 31*, 12483−12490.
(25) Cascella, R., Conti, S., Mannini, B., Li, X., Buxbaum, J. N., Tiribilli, B., Chiti, F., and Cecchi, C. (2013) Transthyretin suppresses the toxicity of oligomers formed by misfolded proteins in vitro. *Biochim. Biophys. Acta 1832*, 2302−2314.
(26) Kelly, J. W. (1996) Alternative conformations of amyloidogenic proteins govern their behavior. *Curr. Opin. Struct. Biol. 6*, 11−17.
(27) Kelly, J. W., Colon, W., Lai, Z., Lashuel, H. A., McCulloch, J., McCutchen, S. L., Miroy, G. J., and Peterson, S. A. (1997) Transthyretin quaternary and tertiary structural changes facilitate misassembly into amyloid. *Adv. Protein Chem. 50*, 161−181.
(28) Nettleton, E. J., Sunde, M., Lai, Z., Kelly, J. W., Dobson, C. M., and Robinson, C. V. (1998) Protein subunit interactions and structural integrity of amyloidogenic transthyretins: Evidence from electrospray mass spectrometry. *J. Mol. Biol. 281*, 553−564.
(29) Serag, A. A., Altenbach, C., Gingery, M., Hubbell, W. L., and Yeates, T. O. (2002) Arrangement of subunits and ordering of β-strands in an amyloid sheet. *Nat. Struct. Biol. 9*, 734−739.
(30) Lim, K. H., Dyson, H. J., Kelly, J. W., and Wright, P. E. (2013) Localized structural fluctuations promote amyloidogenic conformations in transthyretin. *J. Mol. Biol. 425*, 977−988.
(31) Wiseman, R. L., Powers, E. T., and Kelly, J. W. (2005) Partitioning conformational intermediates between competing refolding and aggregation pathways: Insights into transthyretin amyloid disease. *Biochemistry 44*, 16612−16623.
(32) Canet, D., Last, A. M., Tito, P., Sunde, M., Spencer, A., Archer, D. B., Redfield, C., Robinson, C. V., and Dobson, C. M. (2002) Local cooperativity in the unfolding of an amyloidogenic variant of human lysozyme. *Nat. Struct. Biol. 9*, 308−315.
(33) Chiti, F., Mangione, P., Andreola, A., Giorgetti, S., Stefani, M., Dobson, C. M., Bellotti, V., and Taddei, N. (2001) Detection of two partially structured species in the folding process of the amyloidogenic protein β2-microglobulin. *J. Mol. Biol. 307*, 379−391.
(34) Jiang, X., Smith, C. S., Petrassi, H. M., Hammarstrom, P., White, J. T., Sacchettini, J. C., and Kelly, J. W. (2001) An engineered transthyretin monomer that is nonamyloidogenic, unless it is partially denatured. *Biochemistry 40*, 11442−11452.
(35) Palmieri Lde, C., Lima, L. M., Freire, J. B., Bleicher, L., Polikarpov, I., Almeida, F. C., and Foguel, D. (2010) Novel Zn^{2+}-binding sites in human transthyretin: Implications for amyloidogenesis and retinol-binding protein recognition. *J. Biol. Chem. 285*, 31731−31741.
(36) Hurshman Babbes, A. R., Powers, E. T., and Kelly, J. W. (2008) Quantification of the thermodynamically linked quaternary and tertiary structural stabilities of transthyretin and its disease-associated variants: The relationship between stability and amyloidosis. *Biochemistry 47*, 6969−6984.
(37) Hurshman, A. R., White, J. T., Powers, E. T., and Kelly, J. W. (2004) Transthyretin aggregation under partially denaturing conditions is a downhill polymerization. *Biochemistry 43*, 7365−7381.
(38) White, J. T., and Kelly, J. W. (2001) Support for the multigenic hypothesis of amyloidosis: The binding stoichiometry of retinol-binding protein, vitamin A, and thyroid hormone influences transthyretin amyloidogenicity in vitro. *Proc. Natl. Acad. Sci. U.S.A. 98*, 13019−13024.
(39) Hammarstrom, P., Sekijima, Y., White, J. T., Wiseman, R. L., Lim, A., Costello, C. E., Altland, K., Garzuly, F., Budka, H., and Kelly, J. W. (2003) D18G transthyretin is monomeric, aggregation prone, and not detectable in plasma and cerebrospinal fluid: A prescription for central nervous system amyloidosis? *Biochemistry 42*, 6656−6663.
(40) Santoro, M. M., and Bolen, D. W. (1988) Unfolding free energy changes determined by the linear extrapolation method. 1. Unfolding of phenylmethanesulfonyl α-chymotrypsin using different denaturants. *Biochemistry 27*, 8063−8068.
(41) Gianni, S., Ivarsson, Y., Jemth, P., Brunori, M., and Travaglini-Allocatelli, C. (2007) Identification and characterization of protein folding intermediates. *Biophys. Chem. 128*, 105−113.
(42) Jackson, S. E., and Fersht, A. R. (1991) Folding of chymotrypsin inhibitor 2. 1. Evidence for a two-state transition. *Biochemistry 30*, 10428−10435.

(43) Pires, R. H., Karsai, A., Saraiva, M. J., Damas, A. M., and Kellermayer, M. S. (2012) Distinct annular oligomers captured along the assembly and disassembly pathways of transthyretin amyloid protofibrils. *PLoS One 7*, e44992.
(44) Biancalana, M., and Koide, S. (2010) Molecular mechanism of thioflavin-T binding to amyloid fibrils. *Biochim. Biophys. Acta 1804*, 1405−1412.
(45) Kuznetsova, I. M., Turoverov, K. K., and Uversky, V. N. (2004) Use of the phase diagram method to analyze the protein unfolding-refolding reactions: Fishing out the "invisible" intermediates. *J. Proteome Res. 3*, 485−494.
(46) Uversky, V. N., and Fink, A. L. (2004) Conformational constraints for amyloid fibrillation: The importance of being unfolded. *Biochim. Biophys. Acta 1698*, 131−153.
(47) Kelly, S. M., Jess, T. J., and Price, N. C. (2005) How to study proteins by circular dichroism. *Biochim. Biophys. Acta 1751*, 119−139.
(48) Matouschek, A., Kellis, J. T., Jr., Serrano, L., Bycroft, M., and Fersht, A. R. (1990) Transient folding intermediates characterized by protein engineering. *Nature 346*, 440−445.
(49) Ferguson, N., Capaldi, A. P., James, R., Kleanthous, C., and Radford, S. E. (1999) Rapid folding with and without populated intermediates in the homologous four-helix proteins Im7 and Im9. *J. Mol. Biol. 286*, 1597−1608.
(50) Bemporad, F., Capanni, C., Calamai, M., Tutino, M. L., Stefani, M., and Chiti, F. (2004) Studying the folding process of the acylphosphatase from *Sulfolobus solfataricus*. A comparative analysis with other proteins from the same superfamily. *Biochemistry 43*, 9116−9126.
(51) Ternstrom, T., Mayor, U., Akke, M., and Oliveberg, M. (1999) From snapshot to movie: ϕ analysis of protein folding transition states taken one step further. *Proc. Natl. Acad. Sci. U.S.A. 96*, 14854−14859.
(52) Went, H. M., Benitez-Cardoza, C. G., and Jackson, S. E. (2004) Is an intermediate state populated on the folding pathway of ubiquitin? *FEBS Lett. 567*, 333−338.
(53) Bai, Y. (1999) Kinetic evidence for an on-pathway intermediate in the folding of cytochrome c. *Proc. Natl. Acad. Sci. U.S.A. 96*, 477−480.
(54) Haq, S. R., Jurgens, M. C., Chi, C. N., Koh, C. S., Elfstrom, L., Selmer, M., Gianni, S., and Jemth, P. (2010) The plastic energy landscape of protein folding: A triangular folding mechanism with an equilibrium intermediate for a small protein domain. *J. Biol. Chem. 285*, 18051−18059.
(55) Jemth, P., Gianni, S., Day, R., Li, B., Johnson, C. M., Daggett, V., and Fersht, A. R. (2004) Demonstration of a low-energy on-pathway intermediate in a fast-folding protein by kinetics, protein engineering, and simulation. *Proc. Natl. Acad. Sci. U.S.A. 101*, 6450−6455.
(56) Travaglini-Allocatelli, C., Gianni, S., Morea, V., Tramontano, A., Soulimane, T., and Brunori, M. (2003) Exploring the cytochrome c folding mechanism: Cytochrome c552 from *Thermus thermophilus* folds through an on-pathway intermediate. *J. Biol. Chem. 278*, 41136−41140.
(57) Schmid, F. X. (2001) Prolyl isomerases. *Adv. Protein Chem. 59*, 243−282.
(58) Olofsson, A., Ippel, J. H., Wijmenga, S. S., Lundgren, E., and Ohman, A. (2004) Probing solvent accessibility of transthyretin amyloid by solution NMR spectroscopy. *J. Biol. Chem. 279*, 5699−5707.
(59) Serag, A. A., Altenbach, C., Gingery, M., Hubbell, W. L., and Yeates, T. O. (2001) Identification of a subunit interface in transthyretin amyloid fibrils: Evidence for self-assembly from oligomeric building blocks. *Biochemistry 40*, 9089−9096.
(60) Armen, R. S., Alonso, D. O., and Daggett, V. (2004) Anatomy of an amyloidogenic intermediate: Conversion of β-sheet to α-sheet structure in transthyretin at acidic pH. *Structure 12*, 1847−1863.
(61) Li, X., and Buxbaum, J. N. (2011) Transthyretin and the brain re-visited: Is neuronal synthesis of transthyretin protective in Alzheimer's disease? *Mol. Neurodegener. 6*, 79.
(62) Costa, R., Ferreira-da-Silva, F., Saraiva, M. J., and Cardoso, I. (2008) Transthyretin protects against A-β peptide toxicity by proteolytic cleavage of the peptide: A mechanism sensitive to the Kunitz protease inhibitor. *PLoS One 3*, e2899.